Laser-range-finder-based target detection for human-robot collaboration in hilly orchards

Xiulan Bao[1], Xiaojie Ma[1], Yuxin Niu[2], Qilin Yin[1], Hong Chen[1], Qing Wu[1*]

(1. *College of Engineering, Huazhong Agricultural University, Wuhan 430070, China*;
2. *Department of Astronautics Engineering, Harbin Institute of Technology, Harbin, 150001, China*)

Abstract: Human-robot collaboration is a promising means to promote orchard intelligence and reduce the over-reliance on manual work for complex agronomic practices such as fruit tree pruning, flower and fruit thinning, and harvesting. Accurate target detection and recognition of robots on humans are the basis and prerequisite for subsequent autonomous human-robot collaboration. In this study, detection and recognition of following robots for human torso were carried out in a standardized hilly orchard. A LiDAR-based human torso detection method was proposed based on the actual orchard environment. Breakpoint detection was used to cluster and segment the point clouds, and the segmentation thresholds were determined based on experimental results. The geometric attributes of the human torso were trained in the classification detection model, resulting in the extraction of six geometric attributes of the human torso. The classification model was then trained with various combinations to obtain the optimal feature combination [girth-depth-average curvature (*G-D-k*)] for human torso recognition in an orchard environment. Practical experiments were carried out to validate the feasibility and accuracy of the *G-D-k* feature combination. The experimental results demonstrate that the *G-D-k* feature combination can accurately recognize human bodies in orchards. The LiDAR-based detection method can achieve relatively accurate human detection and recognition in complex orchard environments, providing a reference for target detection in human-robot collaboration in orchards.

Keywords: human-robot collaboration, following robot, human torso recognition, LiDAR, support vector data descriptors
DOI: 10.25165/j.ijabe.20251802.8346

Citation: Bao X L, Ma X J, Niu Y X, Yin Q L, Chen H, Wu Q. Laser-range-finder-based target detection for human-robot collaboration in hilly orchards. Int J Agric & Biol Eng, 2025; 18(2): 231–238.

1 Introduction

Orchard management is rather labor-intensive[1], as agronomic practices such as pruning, flower and fruit thinning, and harvesting of evergreen fruit trees such as citrus, litchi, and banana heavily rely on human labor, which can account for about 60% of the production cost[2,3]. To alleviate the constraint of labor costs, several companies and research groups have developed a variety of orchard management robots[4]. However, the performance of these robots is severely limited by the complicated environment and challenging working conditions in orchards because it is challenging for them to identify fruits obscured by leaves, pick fruits inside fruit trees[5], and perform delicate management operations such as fruit tree pruning and flower and fruit thinning[1]. Tri-Co robots can interact with the operating environment, humans, and other robots and can better adapt to unstructured, dynamic environments and understand human behavioral intentions[6,7]. The interaction and cooperation of robots with humans are a prerequisite for human-robot collaboration[8]. The development of human-collaborative robots can greatly improve production efficiency and reduce labor in orchard management, which is crucial for the growth of the fruit industry.

In the human-robot collaboration scenario, autonomous following of the target is the foundation and prerequisite for the collaboration. In previous research, most following robots have been applied to cargo carrying[9,10], tracking shopping carts[11-13], and in the medical industry[14]. Sales et al.[15] designed a shopping cart assistance robot called CompaRob to help older adults carry goods in supermarkets with modularity, simplicity, and ease of use. Guerrero et al.[16] employed the PeTra tool to track pairs of legs in a chaotic environment and verified its accuracy on a public dataset. Feng et al.[17] designed a target-tracking method for human-tracking robots based on ultra-wideband (UWB) technology. Although significant progress has been made in the development and application of following robots in the service industry, the performance of autonomous following algorithms is largely limited by hilly orchard environments and complex and variable interference factors.

Compared with the data collected in an indoor environment, the data acquired in the unstructured environment of an orchard generally include more noise data, which may cause the obscuring or temporary loss of human targets for the following of a mobile robot. In such complicated external environments, following humans remains a great challenge for mobile robots. Following robots have been used in agriculture. Masuzawa et al.[18] employed a mobile robot equipped with an RGB-D camera for the harvesting of flowers in a greenhouse environment, with the RGB-D camera to acquire various information such as color, texture, and depth. Yorozu et al.[19] proposed a human-following control method based on the fuzzy control theory and improved the recognition accuracy

Received date: 2023-05-16 **Accepted date:** 2025-01-06
Biographies: **Xiulan Bao**, PhD, Associate Professor, research interest: agricultural robot, Email: orchidbaoxl@mail.hzau.edu.cn; **Xiaojie Ma**, MS, research interest: human-robot collaboration, Email: mxj3023@163.com; **Yuxin Niu**, PhD candidate, research interest: multibody system dynamics, Email: niuyxhit@163.com; **Qilin Yin**, MS, research interest: agricultural robot, Email: Y931839413@163.com; **Hong Chen**, PhD, Associate Professor, research interest: design and development of orchard operation equipment, Email: chenhong@mail.hzau.edu.cn.
***Corresponding author: Qing Wu**, PhD, Associate Professor, research interest: algorithm optimization. College of Engineering, Huazhong Agricultural University, Wuhan 430070, China. Tel: +86-13659893986, Email: wuqing@mail.hzau.edu.cn.

of the following robot by having the leader wear a red jacket. Polvara et al.[20] achieved accurate localization and tracking of workers in a greenhouse environment by extending a particle filter and combining it with multi-sensor fusion techniques. Mao et al.[21] designed a small orchard transport robot with a dual navigation mode, which uses the OpenPose algorithm to estimate human posture and extract the critical point of the human skeleton center as a target tracking point to achieve pedestrian-led navigation. Although machine vision technology is commonly employed in following robots due to its real-time nature, laser range finder (LRF) has higher robustness for complex and variable outdoor conditions and light intensity.

To enhance the tracking capability of autonomous following robots, many researchers have focused on human target identification. For instance, Taipalus et al.[22] introduced a new algorithm for detecting and tracking human legs. The human leg was scanned with 2D LiDAR and categorized using predetermined conditions for monitoring. Chung et al.[23] employed a single LRF to detect and track human legs, constructed geometric features of human legs, used inductive methods for data association, and then applied Support Vector Data Descriptors (SVDD) to distinguish human legs and other interfering objects. Cha et al.[24] added angular thresholding for point cloud segmentation to extract the human leg region, and used SVDD to learn classification boundaries in the 3D feature space. However, these studies were mostly conducted in hallway and lounge settings, where the noise point cloud is much lower than that in complicated orchard settings. When several persons are in the background, leg detection-based LiDAR may confuse the target with the interfering person and may fail to recognize ladies wearing long skirts. Zainudin et al.[25] analyzed the classification performance of different classifiers in extracting human torso features using 2D LiDAR. Jung et al.[26] used the SVDD model to extract a human torso point cloud and customize the torso geometric attributes to accomplish the autonomous following of a marathon service robot in an outdoor environment. Kim et al.[27] proposed an autonomous following robot system based on a single-line LiDAR and a two-degree-of-freedom balance module to track the human torso on hilly and uneven terrain. In summary, various human detection technologies based on legs and torso have been applied in the field of robot autonomous following. However, in an outdoor orchard environment, the shape of a tree trunk scanned by LiDAR is highly similar to that of human legs, which may lead to the misjudgment of tree trunks as human legs and cause erroneous following. The detection of the human torso can better distinguish humans from fruit trees.

This study proposed a single LiDAR-based target detection method for efficient and accurate control of following robots in orchards. Breakpoint detection and threshold segmentation were combined to achieve clustering segmentation of the human torso point cloud in an orchard environment. In addition, a new optimal feature combination of geometric attributes of the human torso was proposed, whose recognition performance was verified in a real orchard environment.

2 Analysis of orchard environment and operational tasks

2.1 Analysis of the orchard environment

Orchards can be classified as flatland, hilly, or mountainous orchards based on their topography. In China, orchards are predominantly located in hilly and mountainous areas, which account for about 65% of the total orchard area[28]. The hilly orchards are usually dispersed and dominated by terrace or slope planting methods. According to age, they can be primarily divided into traditional orchards and modern standardized orchards. The research object of this study was a standardized hilly citrus orchard (Figure 1). The orchard is located at the experimental base of citrus at Huazhong Agricultural University in Wuhan, Hubei Province. The overall slope of the orchard was about 5°-15°. The citrus trees were planted in a ridge planting pattern with a ridge width of 1.5-2.0 m and a ridge height of 0.2-0.4 m. The spacing between rows of fruit trees was about 3.5-5.0 m, and the interplant distance between fruit trees was approximately 0.8-2.0 m.

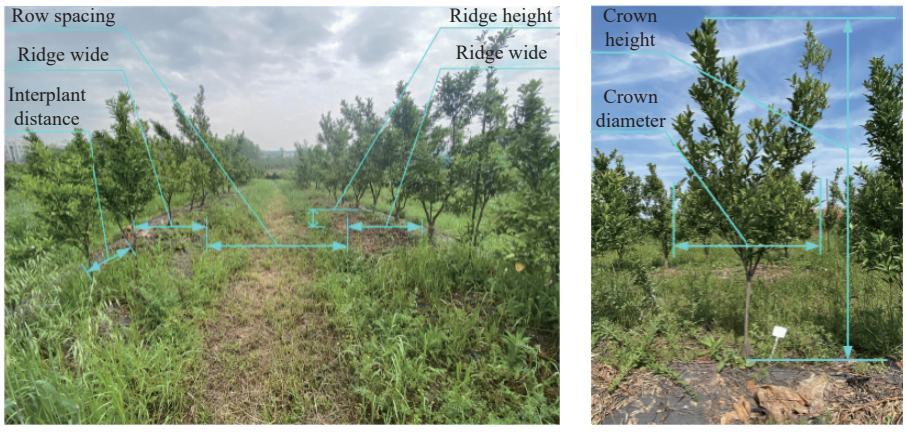

a. Planting pattern of citrus trees in citrus orchards b. Architecture of dwarf citrus trees

Note: The double-headed arrows in the figure indicate the range.

Figure 1 Standardized hilly citrus orchard

Dwarfing is an essential agricultural status quo for modern orchard cultivation and effective management[29]. Dense planting of dwarf citrus trees can realize the planting of wide rows and narrow plant spacing, which can contribute to more fruiting branches and a higher yield. At present, the tree shape of the citrus orchard includes two types of tiny-crown and single-trunk trees, which are all short enough for direct operation of humans without the assistance of ladders (Figure 1b). For the tiny-crown trees, the main trunk height is 35-50 cm; the crown height is 1.5-2.0 m; the crown diameter is ≤2.0 m. The crown has several backbone branches as well as good ventilation and light penetration. For single-trunk trees, the crown height is ≤2.5 m, the crown diameter is ≤1.5 m, and the main trunk

is 40-50 cm, with a uniform distribution of fruiting branches, forming a hedgerow structure. The dense planting mode of dwarf citrus trees is conducive to the combination of agricultural machinery agronomy and mechanized operation to improve production efficiency. Human-robot collaboration can efficiently minimize the labor intensity and expense of some complicated operation tasks such as flower and fruit thinning, pruning, harvesting, and other agronomic procedures.

2.2 Analysis of orchard management tasks

Pruning, flower and fruit thinning, and harvesting are the three most labor-intensive and time-consuming tasks in orchard maintenance (Figure 2). Pruning is meant to manage tree size and structure and reduce crop load during early fruit tree growth. It is currently implemented manually in most orchards. Farmers will determine whether the fruit tree should be pruned based on their examination of the tree structure with their knowledge, skills, and experiences. In addition, flower and fruit thinning can increase fruit setting and fruit quality, minimize nutrient consumption, and achieve steady production of fruit trees through selective removal of tiny or malformed flowers and fruits. Flower and fruit thinning requires precise treatment on each fruiting position of each tree and the selection or removal of each flower by manual operation. Fruit harvesting is a labor-intensive and repetitive operation with high labor costs. Farmers must spend much unproductive time walking and carrying fruit baskets, resulting in a significant waste of labor. The development of collaborative robots can help reduce the labor required by pruning, flower and fruit thinning, and intensive and repetitive harvesting in orchards to improve production efficiency. Here, orchard harvesting was used as an example to study the target detection of human-following robots in orchard practice.

a. Pruning b. Flower and fruit thinning c. Harvesting

Figure 2 Orchard management operations

3 Human torso detection and recognition in orchard human-robot collaboration

3.1 LiDAR point cloud segmentation

Many information points, such as the human torso, leaves, and branches, are included in a point cloud acquired by scanning a frame of 2D LiDAR in an orchard. Figure 3 shows the original point cloud before segmentation. The human torso point cloud is within the red circle, which is flanked by the point clouds of tree trunks and branches, and the red dot represents the coordinate origin of the LiDAR. These point clouds must be divided into clusters so that each cluster includes the same information. The point cloud data are preprocessed before segmentation. The points in the lower half-plane of the LiDAR are filtered out, and the noise points are smoothed by one-dimensional median filtering to improve the computational speed and detection accuracy.

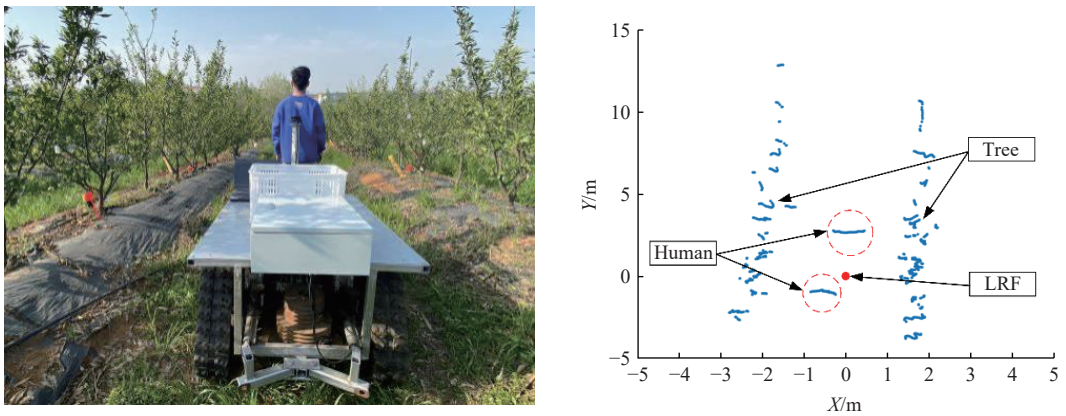

a. Experimental environment b. LRF original point cloud data

Figure 3 Laser range finder (LRF) data in the experimental environment

Given that the point cloud of 2D LiDAR constitutes 2D data (r, θ), the breakpoint detection method is used for point cloud segmentation, which mainly involves the calculation of the distance between two adjacent points. Generally, two points are considered as breakpoints if their distance exceeds the threshold δ. The threshold size can greatly influence the effect of point cloud segmentation, and we here chose δ=20 cm based on the torso point cloud properties. The set threshold divides the n points in each frame of point cloud data into m subsets.

$$P = \{p_1, p_2, \ldots, p_i, \ldots, p_n | p_i = (r_i, \theta_i)\}$$
$$S = \{s_1, s_2, \ldots, s_m\}, s_m = \{p_i, p_{i+1}, \ldots, p_n\} \quad (1)$$

where, P denotes a set of points detected by scanning of a frame by LiDAR; r_i (m) and θ_i (°) represent the distance and angle sensed by the ith laser beam, respectively; s_m denotes the segmented cluster of n points; and S represents a set of segmented point cloud clusters. When the distance d_i between two adjacent points p_i and p_{i+1} is shorter than the threshold δ (m), the two points are classified into one subset; otherwise, the point p_{i+1} is classified into the next subset as

the first point. The iteration is repeated until all points are classified.

3.2 Detection of human torso by SVDD

Due to the complex and dynamic environment of orchards, LiDAR may be misled by interfering objects such as the branches and trunks of fruit trees. AdaBoost and random forest algorithms are commonly used for human detection and classification. The AdaBoost classification algorithm uses the supervised learning method and manually selects some features to complete the classification, but it employs a linear classifier to classify normal and abnormal data, which requires greater classification accuracy. The random forest algorithm is a combined learning approach for generating multiple decision trees as classifiers, and the classification result with the most votes is used as the final classification boundary output. However, this algorithm can produce overfitting in an orchard environment with high disturbance. The SVDD classification algorithm can generate alternative kernel functions to construct different classification boundaries, and the classifier performs better. Therefore, the SVDD classification algorithm is used to distinguish the human torso and other interfering targets. We compared the classification accuracy of several kernel functions and selected the Gaussian kernel function to build the curve classifier for human torso detection. The main principle of SVDD is to map the 2D raw data of LiDAR to the feature space and find a hypersphere with the smallest volume. The optimal feature space is calculated as follows:

$$\begin{aligned} &\min F(R,a,\xi) = R^2 + C\sum_{i=1}^{N}\xi_i \\ &\text{s.t. } \|x_i - a\|^2 \le R^2 + \xi_i,\ \xi_i > 0,\ i = 1,2,\ldots,N \end{aligned} \tag{2}$$

where, ξ_i is the slack variable representing the distance of the data point from the boundary, R is the sphere radius, a is the hypersphere center, and C regulates the trade-off between sphere volume and error. To prevent overfitting of the classification boundary, a small number of negative samples were added to the training set. Assuming that the positive and negative samples in the training set are labeled with y_i=+1 and y_j=−1, respectively, the optimization problem in its original form is transformed into a Lagrange function L denoted as:

$$\begin{aligned} &\min L = \sum_{i=1}^{n}\sum_{j=1}^{n} y_i y_j \alpha_i \alpha_j K(x_i, x_j) - \sum_{i=1}^{n} y_i \alpha_i K(x_i, x_i) \\ &\text{s.t. } \sum_{i=1}^{n} y_i \alpha_i = 1 \end{aligned} \tag{3}$$

where, α_i is the x_i Lagrange coefficient corresponding to the sample, and $K(x_i, y_i)$ is the radial basis function (RBF).

Due to the left and right sway during movement and constant changes in the cloth surface, the human torso shape cannot be characterized as oval or circular. LiDAR was used to scan the torsos of five persons with different heights and body types in an open and unobstructed setting to determine the association between the torso points and collected 1100 sample datasets to train the SVDD model. To ensure the safety of human-robot cooperation, the following range was set at 1-3 m. As a result, the distance between the subject's torso and the LRF in the sample data is 1-3 m, and the LiDAR scanning height is 1.1 m.

Six attributes were defined to describe the shape of the torso LRF data, as shown in Figure 4.

G denotes the girth feature of the torso LRF clustering data, which is obtained by superimposing the distances between two adjacent points in the torso data with the following equation:

$$G = \sum_{i=1}^{n-1} |p_i p_{i+1}| \tag{4}$$

where, W denotes the clustered data of torso width. W is defined as the distance between the two endpoints of the torso data and expressed as follows:

$$W = |p_1 p_n| \tag{5}$$

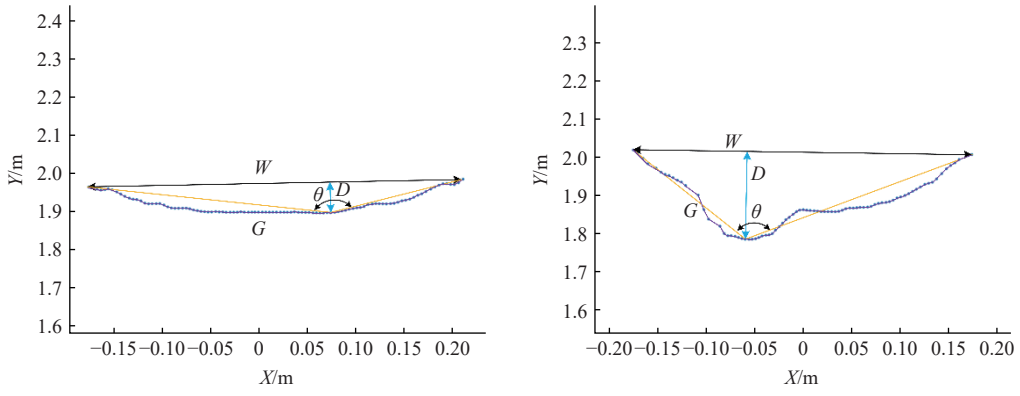

a. Human back torso point cloud b. Human side torso point cloud

Note: G denotes the arc length of the human torso (m); W denotes the width of the human torso (m); D denotes the depth of the human torso (m); and θ denotes the angle of the human torso (°).

Figure 4 Human torso point cloud attributes

D represents the depth feature of the torso data and is defined as the maximum distance from the point on the torso to the line connecting the two endpoints as follows:

$$D = \left(\frac{\left|\overrightarrow{p_1 p_n} \times \overrightarrow{p_1 p_i}\right|}{|p_1 p_n|} \right)_{\max} \tag{6}$$

$\bar{k}$ denotes the average curvature of the torso. Three consecutive points x_A, x_B, and x_C are defined on the segment, and A is used to denote the area of the triangle formed by $x_A x_B x_C$, and d_A, d_B, and d_C indicate the length of the three sides of the triangle, respectively. The discrete curvature k_i at x_B is approximated as:

$$\begin{aligned} &\bar{k} = \sum_{i=1}^{n-2} k_i \\ &k_i = \frac{4A}{d_A d_B d_C} \end{aligned} \tag{7}$$

θ represents the angle of the torso data, and is defined as the angle formed between the lines connecting the farthest point to the first point and the last point, as represented by the following equation:

$$\theta = \arccos \frac{|p_i p_1| \times |p_i p_n|}{\left|\overrightarrow{p_i p_1}\right| \times \left|\overrightarrow{p_i p_n}\right|} \tag{8}$$

In addition, the ratio of torso width was defined to girth as a new feature to describe the degree of circularity of the clustered data.

The above six geometric attributes are combined into different feature vectors, and the feature vectors of each cluster are labeled. The torso segments are labeled as positive samples, and other segments are labeled as negative samples, which are input into the SVDD model for training to generate the classification boundary. As shown in Figure 5, all clustered data inside the boundary are considered human torso data, and those outside the boundary are considered non-human data.

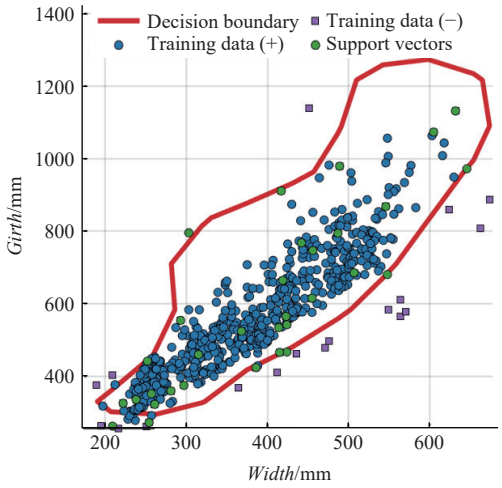

Figure 5 SVDD training boundary

4 Experiments

4.1 Following robot-assisted picking in orchard

The robot utilized to assist in picking is shown in Figure 6. The following robot consists of a power supply system, a drive system, and a control system. The LiDAR is mounted on the centerline of the following robot at a height of 1.1 m from the ground. The SLAMTEC RPLiDAR S2 from Silan is selected for the LiDAR, with a 360° scanning area, a resolution of 0.12°, and a scanning distance of 30 m. The parameters of the following robot are listed in Table 1, and the LiDAR specifications are listed in Table 2.

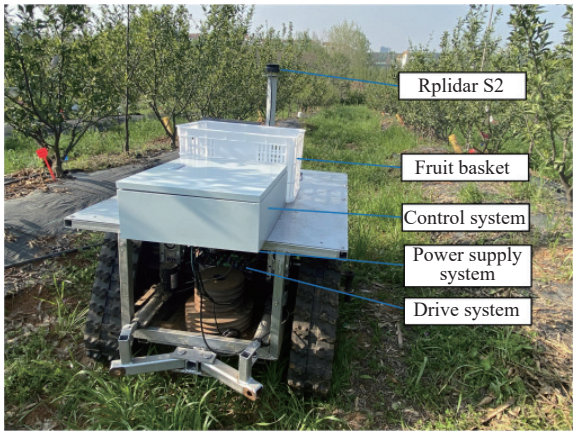

Figure 6 Following robot for assistance in picking

Table 1 Parameters of the following robot

Description	Parameter
Dimension L×W×H/mm×mm×mm	1200×900×60
Width between tracks/mm	900
Track length/mm	1200
Power supply	48 V Lithium battery
Battery life/h	About 2 h

Table 2 Parameters of laser ranging sensor

Description	Parameter
Distance measuring method	Time-of-flight ranging (TOF)
Measuring radius	White object (m): 0.05-30.00 Black object (m): 0.05-10.00
Measuring range	360°
Ranging accuracy	±5 cm
Angular resolution	0.12°
Sampling frequency	32 kHz

4.2 Results of point cloud clustering segmentation for LiDAR

We performed clustering segmentation on point clouds scanned by LiDAR in outdoor situations to evaluate the adaptability of the clustering segmentation algorithm to challenging contexts. Figure 7 shows the segmented point cloud data. The five central segments are five human torso point cloud data for clustering segmentation, while those on both sides are the wall point cloud data for clustering segmentation. The segmentation threshold parameters are manually modified based on the segmentation effect, and the threshold value is set to δ = 20 cm.

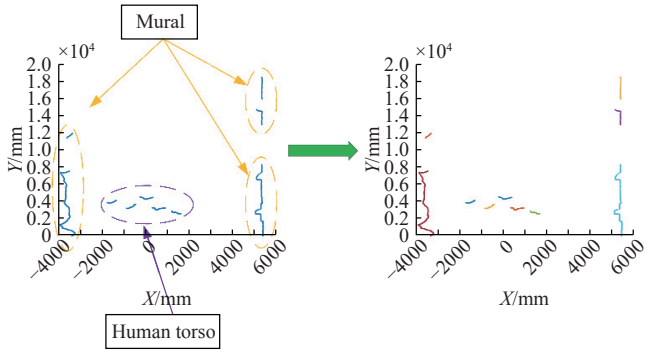

Figure 7 Point cloud segmentation results in outdoor environment

4.3 Results of SVDD classification in the orchard environment

LRF data were obtained from the orchard environment, combining different features and the optimal feature combination for human torso recognition by testing the SVDD classifier. Many leaves and branches in the actual orchard setting resemble the shape of the human torso, and we identified this information as other distractor information. First, 2188 clustered datasets were obtained in 120 consecutive frames of scanned data, including 1987 human torso datasets and 199 other distractor datasets. Then, feature extraction was performed on these clustered data and each of the torso attributes was calculated. Finally, different combinations of these features were used to train and test the SVDD model, where the ratio of the training set to the test set is 7:3. By analyzing the sample data, the range of each feature of the human torso and non-human torso was obtained as listed in Table 3.

In the classification and detection model, relying solely on accuracy may lead to misinterpretation. Therefore, in this study, the Receiver Operating Characteristic (ROC) curve was plotted and the Area Under the Curve (AUC) was calculated as the evaluation criterion to assess the recognition performance under different

feature combinations. To calculate the value of AUC, sensitivity (TPR) and specificity (FPR) were introduced. The sensitivity represents the proportion of all human torso samples that are correctly predicted, and the specificity represents the proportion of all non-human torso samples that are incorrectly predicted as human torsos, which are specifically expressed as follows:

$$\mathrm{TPR} = \frac{\mathrm{TP}}{\mathrm{TP} + \mathrm{FN}} \tag{9}$$

$$\mathrm{FPR} = \frac{\mathrm{FP}}{\mathrm{FP} + \mathrm{TN}} \tag{10}$$

where, TP represents the number of positive samples detected correctly, FP represents the number of positive samples detected incorrectly, FN represents the number of negative samples detected incorrectly, and TN represents the number of negative samples detected correctly.

The AUC is calculated by integration:

$$\mathrm{AUC} = \int_0^1 \mathrm{TPR} d(\mathrm{FPR}) \tag{11}$$

In the discrete case, the AUC can be approximately calculated by the trapezoidal method:

$$\mathrm{AUC} \approx \sum_{i=1}^{n-1} (\mathrm{FPR}_{i+1} - \mathrm{FPR}_i) \frac{\mathrm{TPR}_i + \mathrm{TPR}_{i+1}}{2} \tag{12}$$

Table 3 Comparison of the range of each feature for human and non-human torsos

Type	Girth/ mm	Width/ mm	Depth/ mm	Average curvature	Angle/ (°)	Width/ Girth
Human torso	[162, 1567]	[113, 1283]	[18, 422]	[0.0717, 39.306]	[48.095, 164.33]	[0.3173, 0.9763]
Non-human torso	[28, 3558]	[25, 1361]	[0, 426]	[0.0017, 15.707]	[30.512, 178.92]	[0.2865, 0.9999]

The results of SVDD model detection for different feature combinations are shown in Table 4. The first row in Table 4 presents different feature combinations: *G* represents the girth; *W* represents the width; *D* denotes the depth; *k* means the average curvature; *A* means the angle; and *B* represents the width/girth ratio. The model's training set accuracy and test set accuracy are shown in the second and third rows, respectively. The last row indicates the AUC value for each combination of features.

Table 4 SVDD classification results for different feature combinations

Index	*G-B*	*W-D*	*G-W-D*	*G-W-A*	*G-D-A*	*W-A-B*	*G-W-k*	*G-D-k*
Accuracy of training set/%	72.59	94.76	95.16	95.09	95.16	94.50	98.69	95.68
Accuracy of test set/%	73.36	92.99	93.60	92.69	93.30	93.91	89.00	93.60
AUC	0.5003	0.8556	0.8250	0.8499	0.8266	0.8149	0.8275	0.8748

Note: *G* represents the girth (m); *W* represents the width (m); *D* denotes the depth (m); *k* means the average curvature; *A* means the angle (°); and *B* represents the width/girth ratio. Same below.

In the performance evaluation process, a larger value of AUC indicates a better human torso detection performance with this feature combination. According to the training and test accuracy, the use of multiple features in SVDD is relatively more effective. As the number of feature combinations increases, the detection performance of the model is enhanced, while the computational complexity is higher, and the model training time is longer. Therefore, combining judgment of feature variability, detection performance, and computational complexity of model training and testing, we chose the girth-depth-average curvature (*G-D-k*) feature combination to detect the human torso. The classification boundary of the optimal feature combination is shown in Figure 8. A positive sample is represented by the blue diamond square, which means human torso data and other interfering data classified as negative samples are represented by the orange square. Support vector data are shown in yellow circles. The light blue-green color indicates the classification boundary trained by using SVDD. Since the majority of negative samples in the orchard are branches and trunks, the negative examples are primarily concentrated in the 100 mm× 1000 mm cube in Figure 8.

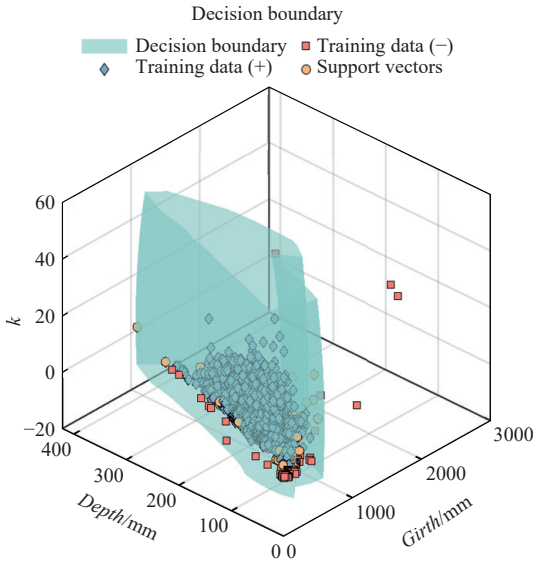

Note: *k* is the average curvature. Same below.

Figure 8 Classification boundaries for optimal feature combinations

The proposed torso-based human detection method was compared with the leg-based human detection method. The comparison results are listed in Table 5. It can be known from the recognition accuracy that the method proposed in this study has a better effect compared with other methods. There are two segments in the human leg point cloud data. Due to the randomness of human body movements, the leg point cloud data is prone to problems such as association errors and occlusion losses. In the orchard environment, the detection method based on legs is likely to identify objects such as tree trunks and cylindrical obstacles as human legs, resulting in incorrect following. Therefore, in the complex environment of the orchard, the detection method based on the human torso has a better effect.

Table 5 Comparison results of different human detection methods

Human body detection parts	Detection methods	Accuracy/%
Human torso	Method proposed in this study	95.68
	G-W feature combination method[27]	83.00
Human legs	Heuristic detection method[22]	77.80
	G-W feature combination method[23]	85.60
	G-W-D feature combination method[24]	89.80

To verify the performance of SVDD classification with the optimal feature combination, we selected different kinds of point cloud clustering information in the orchard environment, as shown in Figure 9, mainly including the human torso, electric cabinet, branches, and leaves. The LRF data were clustered and segmented to construct a clustered dataset, and features were extracted. As shown in Figure 9a, leaves and branches of the fruit tree are the

most frequent disturbance on following robots in orchards. The leaves and/or trunks are connected to form point clouds with similar shapes to the human torso. Therefore, we extracted the point clouds of leaves and branches, as shown in Figures 9b-9c, to analyze the differences in geometric properties between leaves/branches and human torso. Point cloud data extraction was also performed for obstacles such as electrical cabinets and display screens that appear randomly in the orchard, as shown in Figures 9d-9h. The clustered LRF data were extracted based on the defined features, and the results are listed in Table 6.

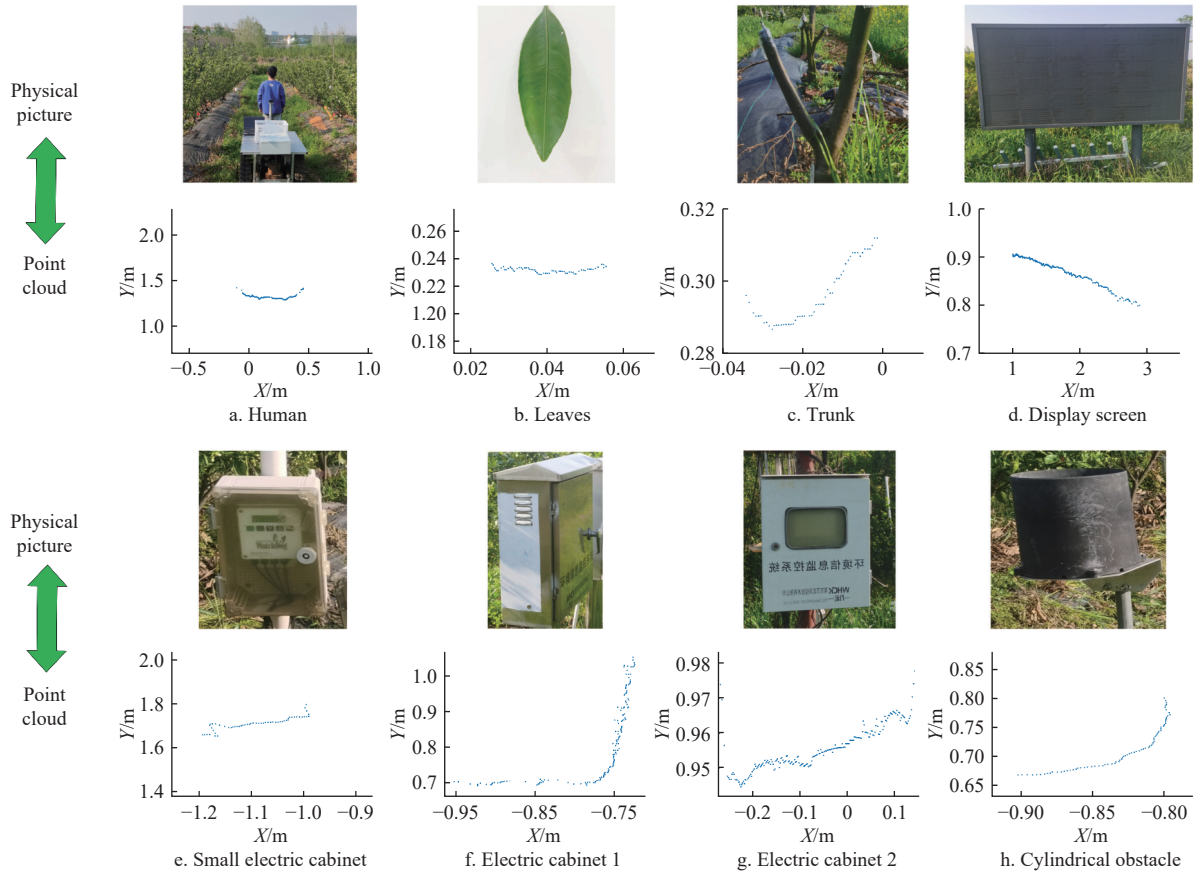

Figure 9 Different objects in the orchard and the corresponding LRF data

The training boundaries obtained from the optimal feature combination were used to determine whether the clustered data belonged to the human torso. The results in Figure 10 show that the human torso data are inside the boundary, and the interfering data are all outside the boundary, indicating that the feature combination can distinguish the interfering clustering data from those of humans.

Table 6 Different kinds of LRF clustering feature data

Index	Human	Electric cabinet 1	Electric cabinet 2	Display screen	Small electric cabinet	Cylindrical obstacle	Citrus leaves	Citrus trunk
G/mm	632	683	478	1914	354	199	59	58
D/mm	143	261	30	13	22	43	6	12
k	2.6481	22.2894	35.6407	7.7085	3.5874	8.992	45.7331	24.2839

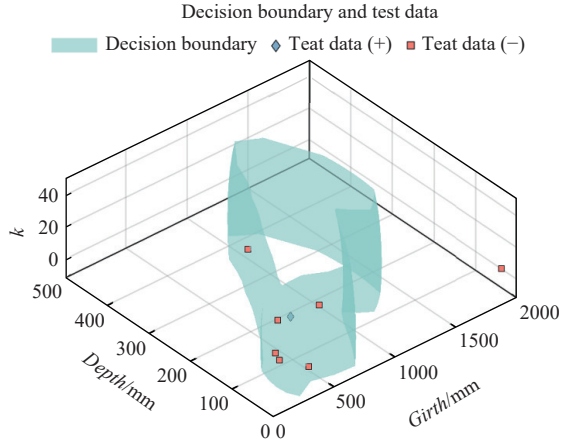

Figure 10 Human torso and interferer data differentiation

5 Conclusions

In this study, a target detection method of following robots was proposed for the human torso in an orchard environment using a single-line LiDAR range finder. Compared with the following method based on scanning and correlation to human legs, the proposed target detection method has more significant differentiation and better detection effect in a cluttered orchard environment. The point cloud data acquired by the 2D LiDAR deployed at the human torso position can be segmented by clustering using the breakpoint detection method. The segmentation threshold is set as δ=20 cm according to the properties of the torso point cloud, whose reliability was verified by experiments. Six geometric attributes were extracted from the human torso, and the SVDD classification model was used to explore alternative feature combinations. Finally, girth-depth-average curvature (*G*-*D*-*k*) was identified as the optimal feature combination with a recognition accuracy of 95.68%. This feature combination was evaluated in a real orchard environment, and the experimental results demonstrated that it could accurately distinguish between humans and disturbances. This method can provide a reference for the target detection of following robots in orchards.

Acknowledgements

This work was funded by the Agricultural Machinery Equipment Weak Core Technology Application Project of Hubei Province, China (Grant No. HBSNYT202219), Nature Science Foundation of Hubei Province, China (Grant No. 2021CFB471), and the National Key Research and Development Program of China (Grant No. 2020YFD1000100).

[References]

[1] Yuan B, Chen C. Evolution of a development model for fruit industry against background of rising labor cost: Intensive or extensive adjustment? Sustainability, 2019; 11(14): 3864.

[2] Mao W J, Liu H, Hao W, Yang F Z, Lin Z J. Development of a combined orchard harvesting robot navigation system. Remote Sensing, 2022; 14(3): 675.

[3] Silwal A, Davidson J R, Karkee M, Mo C, Zhang Q, Lewis K. Design, integration, and field evaluation of a robotic apple harvester. Journal of Field Robotics, 2017; 34(6): 1140–1159.

[4] Verbiest R, Ruysen K, Vanwalleghem T, Demeester E, Kellens K. Automation and robotics in the cultivation of pome fruit: Where do we stand today? Journal of Field Robotics, 2021; 38(4): 513–531. doi: 10.1002/rob.22000.

[5] Tang Y C, Chen M Y, Wang CL, Luo, L F, Li J H, Lian G P, et al. Recognition and localization methods for vision-based fruit picking robots: A review. Frontiers in Plant Science, 2020; 11: 510.

[6] Ding H, Yang X, Zheng N, Li M, Lai Y, Wu H. Tri-Co Robot: A Chinese robotic research initiative for enhanced robot interaction capabilities. National Science Review, 2018; 5(6): 799–801.

[7] Wang G, Li W L, Jiang C, Zhu D H, Xie H, Liu X J. Simultaneous calibration of multicoordinates for a dual-robot system by solving the AXB=YCZ problem. IEEE Transactions on Robotics, 2021; 37(4): 1172–1185.

[8] Lai Y N, Ye X, Ding H. Research progress of major research plan on Tri-Co robots. Journal of Mechanical Engineering, 2021; 57(23): 1–11, 20. (in Chinese)

[9] Hirose N, Tajima R, Sukigara K. Personal robot assisting transportation to support active human life—Human-following method based on model predictive control for adjacency without collision. In: 2015 IEEE International Conference on Mechatronics (ICM), Nagoya: IEEE, 2015; pp.76–81. doi: 10.1109/ICMECH.2015.7083951.

[10] Gupta M, Kumar S, Behera L, Subramanian V. A novel vision-based tracking algorithm for a human-following mobile robot. IEEE Transactions on Systems, Man, and Cybernetics: Systems, 2016; 47(7): 1415–1427.

[11] Alves R, Linhares B, Souza J. Autonomous shopping cart: A new concept of service robot for assisting customers. In: 2018 Latin American Robotic Symposium, 2018 Brazilian Symposium on Robotic (SBR) and 2018 Workshop on Robotics in Education (WRE), João Pessoa: IEEE, 2018; pp.451–456. doi: 10.1109/LARS/SBR/WRE.2018.00086.

[12] Su H, Zhang Y S, Li J S, Hu J. The shopping assistant robot design based on ROS and deep learning. In: 2016 2nd International Conference on Cloud Computing and Internet of Things. Dalian: IEEE, 2016; pp.173–176. doi: 10.1109/CCIOT.2016.7868328.

[13] Gross H, Meyer S, Scheidig A, Eisenbach M, Mueller S, Trinh T, et al. Mobile robot companion for walking training of stroke patients in clinical post-stroke rehabilitation. In: 2017 IEEE International Conference on Robotics and Automation (ICRA), Singapore: IEEE, 2017; pp.1028–1035. doi: 10.1109/ICRA.2017.7989124.

[14] Xiao H Z, Li Z J, Yang C G, Yuan W, Wang L Y. RGB-D sensor-based visual target detection and tracking for an intelligent wheelchair robot in indoors environments. International Journal of Control, Automation and Systems, 2015; 13: 521–529.

[15] Sales J, Martí J, Marín R, Cervera E J, Sanz P. CompaRob: The shopping cart assistance robot. International Journal of Distributed Sensor Networks, 2016; 12(2): 4781280.

[16] Guerrero-Higueras Á, Álvarez-Aparicio C, Calvo Olivera M, Rodríguez-Lera F, Fernández-Llamas C, Rico F, et al. Tracking people in a mobile robot from 2d lidar scans using full convolutional neural networks for security in cluttered environments. Frontiers in Neurorobotics, 2019; 12: 85.

[17] Feng T, Yu Y, Wu L, Bai Y R, Xiao Z, Lu Z. A human-tracking robot using ultra wideband technology. IEEE Access, 2018; 6: 42541–42550.

[18] Masuzawa H, Miura J, Oishi S. Development of a mobile robot for harvest support in greenhouse horticulture—Person following and mapping. In: 2017 IEEE/SICE International Symposium on System Integration. Taipei: IEEE, 2017; pp.541–546. doi: 10.1109/SII.2017.8279277.

[19] Yorozu A, Ishigami G, Takahashi M. Human-following control in furrow for agricultural support robot. In: Intelligent Autonomous Systems 16: Proceedings of the 16th International Conference IAS-16, Cham: Springer, 2022; pp.155–164. doi: 10.1007/978-3-030-95892-3_12.

[20] Polvara R, Del Duchetto F, Neumann G, Hanheide M. Navigate-and-seek: A robotics framework for people localization in agricultural environments. IEEE Robotics and Automation Letters, 2021; 6(4): 6577–6584.

[21] Mao W J, Liu H, Wang X L, Yang F Z, Liu Z J, Wang Z Y. Design and experiment of dual navigation mode orchard transport robot. Transactions of the CSAM, 2022; 53(3): 27–39, 49. (in Chinese)

[22] Taipalus T, Ahtiainen J. Human detection and tracking with knee-high mobile 2D LIDAR. In: 2011 IEEE International Conference on Robotics and Biomimetics, Karon Beach: IEEE, 2011; pp.1672–1677. doi: 10.1109/ROBIO.2011.6181529.

[23] Chung W, Kim H, Yoo Y, Moon C, Park J. The detection and following of human legs through inductive approaches for a mobile robot with a single laser range finder. IEEE Transactions on Industrial Electronics, 2012; 59(8): 3156–3166.

[24] Cha D, Chung W. Human-leg detection in 3D feature space for a person-following mobile robot using 2D LiDARs. International Journal of Precision Engineering and Manufacturing, 2020; 21: 1299–1307.

[25] Zainudin Z, Kodagoda S, Dissanayake G. Torso detection and tracking using a 2d laser range finder. In: Proceedings of the 2010 Australasian Conference on Robotics and Automation, ACRA 2010, 2010. Available: https://opus.lib.uts.edu.au/bitstream/10453/16405/1/2010000410.pdf. Accessed on [2022-12-07].

[26] Jung E, Lee J, Yi B, Park J, Yuta S, Noh S. Development of a laser-range-finder-based human tracking and control algorithm for a marathoner service robot. IEEE/ASME Transactions on Mechatronics, 2013; 19(6): 1963–1976.

[27] Kim J, Jeong H, Lee D. Single 2D lidar based follow-me of mobile robot on hilly terrains. Journal of Mechanical Science and Technology, 2020; 34: 3845–3854.

[28] Zheng Y J, Chen B T, Lyu H D, Kang F, Jiang S J. Research progress of orchard plant protection mechanization technology and equipment in China. Transactions of the CSAE, 2020; 36(20): 110–124. (in Chinese)

[29] Hayat F, Li J, Iqbal S, Peng Y, Hong L M, Balal R, et al. A mini review of citrus rootstocks and their role in high-density orchards. Plants, 2022; 11(21): 2876.